Viscosity Corrections for Concentrated Suspension in Capillary Flow with Wall Slip

Z. Y. Wang
The School of Mechanical and Aerospace Engineering, Nanyang Technological University, Singapore 639798, Singapore

Y. C. Lam
The School of Mechanical and Aerospace Engineering, Nanyang Technological University, Singapore 639798, Singapore

Singapore-MIT Alliance Programme, Nanyang Technological University, Singapore 639798, Singapore

X. Chen
Singapore-MIT Alliance Programme, Nanyang Technological University, Singapore 639798, Singapore

S. C. Joshi
The School of Mechanical and Aerospace Engineering, Nanyang Technological University, Singapore 639798, Singapore

DOI 10.1002/aic.12095
Published online October 29, 2009 in Wiley InterScience (www.interscience.wiley.com).

Corrections for viscosity measurements of concentrated suspension with capillary rheometer experiments were investigated. These corrections include end effects, Rabinowitsch effect, and wall slip. The effects of temperature, particle concentration, and contraction ratio on the end effects were studied and their effects were accounted for using an entrance and exit losses model. The non-Newtonian effect and the nonlinearity of slip velocity against wall shear stress were described using a slip model. The true viscosity of a concentrated suspension with glass powder suspended in a non-Newtonian binder system was calculated as a function of shear rate and effective particle concentration, taking into consideration particle migration, which is calculated by a diffusive numerical model. Particle size was found to affect significantly the viscosity of the suspension with viscosity decreasing with increasing particle size, which can be reflected by a decrease in the value of the power-law index in the Krieger model. © 2009 American Institute of Chemical Engineers *AIChE J,* 56: 1447–1455, 2010
Keywords: viscosity, corrections, concentrated suspension, wall slip, particle migration

Introduction

Polymers filled with inorganic particles have received attention as a result of their industrial and commercial relevance.[1] An important characteristic of these systems are their viscosities, which are generally measured using a capillary viscometer. A number of factors can affect the measured viscosity and introduce errors in the measurements. To improve the accuracy of the measurement, various corrections are made to the experimentally obtained data.

One of the important corrections is the end effect correction. The converging and diverging streamlines at the entrance and exit of the capillary must be taken into consideration for

Correspondence concerning this article should be addressed to Y. C. Lam at myclam@ntu.edu.sg
Z. Y. Wang is also currently affiliated with the Singapore-IT Alliance Programme.

accurate calculation of viscosity from capillary viscometers. The entrance and exit losses, ΔP_e, can be calculated from a Bagley plot showing capillary pressure drop vs. the ratio of die length to radius (L/R), with apparent wall shear rate as a parameter.[2] If a linear Bagley plot, ΔP_e can be calculated directly by linear curve fitting. However, in many cases, a Bagley plot deviates from linearity due to the dependence of viscosity on pressure and/or wall slip. If the viscosity is dependent on pressure, the Bagley plot exhibits an upward curvature.[3] With slip velocity decreasing with hydraulic pressure, the shear rate will depend on the axial position in the channel, which results in a concave Bagley plot.[4] For a nonlinear Bagley, polynomial curve fitting is required to calculate the entrance and exit losses.

In addition to the end effects, to obtain the true viscosity of a concentrated suspension with particles dispersed in a non-Newtonian binder system, two additional corrections should also be considered, i.e., Rabinowitsch correction for a non-Newtonian fluid[5] and slip correction to account for wall slip which results in a higher flow rate.

Apparent slip mechanism is commonly accepted for a concentrated suspension. This mechanism may be ascribed to the formation of a generally relatively thin layer of polymer melt (with deprivation of particles) adjacent to the wall due to the migration of particles from the layer to the centre or the inability of particles to pack at the wall as efficiently as they can away from the wall.[6,7] There are many experiments showing particle migration from high-shear rate region (near the wall) to low-shear rate region (the centre) in a nonhomogeneous shear flow of a concentrated suspension.[8–10]

Particle migration and wall slip are closely interrelated. The nonuniform particle concentration due to shear-induced particle migration can affect the effective viscosity of a concentrated suspension as well as the slip coefficient in a significant way.[11] Theoretically, particle migration could be described by a phenomenological model, which assumes that there are two primary causes for particle migration, namely particle interaction and local variations of concentration-dependent viscosity.[12–14]

The slip velocity in a capillary flow is generally determined using Mooney method by changing the surface-to-volume ratio of the capillary die.[15] Yilmazer and Kalyon[16] and subsequently Kalyon[6,17] provided the analysis and the associated expressions for the determination of the true wall shear rate in capillary flow of concentrated suspension with wall slip correction. Besides Mooney method, Oldroyd[18] or Jastrzebski method[19] was proposed for a concentrated suspension, but these methods were criticized as empirical expressions for their lacking of a coherent physical justification.[20]

Hitherto, there are few studies on the combined effects of particle migration, wall slip, non-Newtonian viscosity, and end effects on viscosity measurements in capillary rheometry. This study presents a systematic investigation on these effects for obtaining the true viscosity of a concentrated suspension.

Theoretical Formulations

Viscosity of concentrated suspension

A bulk suspension stress can be written in two parts, namely stresses from the bulk fluid binder system and the particle system, i.e. $\sigma = \sigma_f + \sigma_p$. The fluid phase stress is assumed to be[21]:

$$\sigma_f = -P\mathbf{I} + 2\eta_b\mathbf{E} \tag{1}$$

where P is the fluid phase averaged pressure, $\mathbf{I}$ is the identity tensor, η_b is the viscosity of a suspending fluid, and $\mathbf{E}$ is the local rate of strain defined as[21]:

$$\mathbf{E} = \frac{1}{2}\left[\nabla\bar{u} + \nabla\bar{u}^T\right] \tag{2}$$

where $\bar{u}$ is the velocity field.

The constitutive law for the particle stress in the absence of the normal stress portion is given as[22]:

$$\sigma_p = 2\eta_b\eta_p(\phi)\mathbf{E} \tag{3}$$

Thus, the bulk suspension stress can be expressed as[23]:

$$\sigma = \sigma_f + \sigma_p = -P\mathbf{I} + 2\eta_b\lfloor 1 + \eta_p(\phi)\rfloor\mathbf{E} = -P\mathbf{I} + 2\eta\mathbf{E} \tag{4}$$

where $\eta = \eta_b\lfloor 1 + \eta_p(\phi)\rfloor$ is a particle concentration dependent shear viscosity. This viscosity can be modeled in a number of different forms.[24] The Krieger model, which describes a shear deformation and concentration dependent viscosity, is adopted[25]:

$$\eta = \eta_b\left(1 - \frac{\phi}{\phi_c}\right)^{-m} \tag{5}$$

where m is a material constant, ϕ and ϕ_c are effective particle concentration and critical loading respectively of a concentrated suspension.

This rheological model describes the effect of the volume fraction of the powder on the flow behavior of a powder/binder mixture, which can be applied to a concentrated suspension. The viscosity of the binder can be described by a modified Cross model with shear-thinning effect[5]:

$$\eta_b = \frac{\eta_0}{1 + (\eta_0\dot{\gamma}/\tau^*)^{1-n}} \tag{6}$$

where η_0 is the Newtonian viscosity at zero shear-rate or approximated by a sufficient small shear rate $\dot{\gamma}$, n is the flow index, $\eta_0 = A\exp(T_b/T)$, where A and T_b are material constants. τ^* is a stress parameter. At high-shear rate, Eq. 6 can be simplified to a power-law model:

$$\eta_b = \left(\eta_0\dot{\gamma}_0^{1-n}\right)\dot{\gamma}^{n-1} \tag{7}$$

where $\dot{\gamma}_0 = \tau^*/\eta_0$ with unit of 1/s.

Particle migration

A diffusive flux model was developed to predict the concentration profile based on a Newtonian binder system[13]:

$$\frac{D\phi}{Dt} = -\nabla\cdot\left(N_c + N_\eta + N_b\right) \tag{8}$$

$$N_c = -k_c a^2\phi\nabla(\phi\dot{\gamma}) \tag{9}$$

$$N_\eta = -k_\eta\phi^2\dot{\gamma}\left(\frac{a^2}{\eta}\right)\nabla\eta \tag{10}$$

$$N_b = -D\nabla\phi \tag{11}$$

where $D/Dt = \partial/\partial t + \overline{u}\cdot\nabla$ is the material derivative, $\overline{u}$ is the velocity of suspension flow, k_c and k_η are two phenomenological parameters. N_c accounts for the effect of the spatially varying interaction frequency, N_η describes the effect of the spatially varying viscosity, and N_b accounts for the Brownian diffusion of particles.

If the particle Peclet number $P_e = a^2\dot{\gamma}/H$, defined in terms of the local shear rate $\dot{\gamma}$, particle radius a, and the diffusivity H, is large for a concentrated suspension flowing in a capillary rheometer, i.e. $a^2\dot{\gamma} \gg H$, the term $H/a^2\dot{\gamma}$ (associated with Brownian motion) in Eq. 8 is very small (i.e., $\frac{H}{a^2\dot{\gamma}} \ll k_c\phi$) and can be neglected.

As the migration effect of particles is dependent on the viscosity, the viscosity effect can be assumed to be a lumped concentration effect.[26] Thus, Eq. 8 can be simplified to:

$$\frac{D\phi}{Dt} = \nabla\cdot\left[k_c a^2\phi\nabla(\phi\dot{\gamma}) + k_\eta a^2\phi^2\dot{\gamma}\left(\frac{\nabla\eta}{\eta}\right)\right] \tag{12}$$

Graham et al.[27] suggested that k_c is a concentration-dependent parameter due to multibody interactions of particles, while k_η is a constant. The values of k_c and k_η were determined initially by statistical calculation based on experimental data on a generalized-Newtonian fluid[28]:

$$k_c = 0.85\phi k_\eta \tag{13}$$

$$k_\eta = 0.59 \tag{14}$$

The boundary condition of no particle flux through the wall of a cylindrical tube has to be enforced:

$$\left(k_c\phi\nabla(\phi\dot{\gamma}) + k_\eta\phi^2\dot{\gamma}\frac{\nabla\eta}{\eta}\right)\cdot n = 0 \tag{15}$$

The zero flux condition applies not only on solid walls but also on surfaces of symmetry. The particle concentration ϕ is assumed to be uniform initially at the entrance of the tube and can be expressed as:

$$\phi = \phi_0, 0 \le r \le R, \text{at } z = 0 \tag{16}$$

The details for solving the coupled flow and diffusive equations are described in Appendices A and B.

Entrance and exit losses model

Jastrzebski[19] proposed a power-law function to correlate the entrance and exit losses, ΔP_e, with the volumetric flow rate, Q, as:

$$\Delta P_e = Be^{cR}Q^p \tag{17}$$

where B is a characteristic constant for a given concentration, c is a constant related to die radius R, p is the flow index.

However, there are some limitations in expression (17). First, in the entrance and exit losses, entrance loss plays a major role. As entrance loss is basically the pressure drop due to the converging flow from the large reservoir to the small capillary, it should be related to the contraction of diameters between the barrel and the capillary, and not only on the capillary die radius. Second, Jastrzebski[19] did not consider the effect of temperature. Experimental results showed that temperature affects the constant p. Thus, we modified the entrance and exit losses expression as[29]:

$$\Delta P_e = f(\phi)\left(\frac{D}{D_{barrel}}\right)^z Q^{f(T)} \tag{18}$$

where D and D_{barrel} are capillary diameter and barrel diameter, respectively. T is temperature.

The functions $f(\phi)$, $f(T)$, and index z can be obtained by correlation with experimental data using expression (18) in three separate steps:

1. Calculate $f(T)$ with the entrance and exit losses at the same contraction ratio and the same particle concentration but at different temperatures;
2. Calculate the value of z based on the entrance and exit losses at the same temperature and with the same particle concentration;
3. $f(\phi)$ can be calculated with the entrance and exit losses with the same contraction ratio and at the same temperature for concentrated suspensions with different particle concentrations.

Wall slip

Being a two-phase system, many suspensions show a characteristic slippage at the wall surface.[30] By applying Leibnitz rule of differentiation with wall slip, the Yilmazer and Kalyon[16] equation for the true shear rate at the wall can be derived:

$$\dot{\gamma}_w = \left(\frac{Q - \pi R^2 u_s}{\pi R^3}\right)\left[3 + \frac{d\ln[(Q - \pi R^2 u_s)/\pi R^3]}{d\ln\tau_w}\right] \tag{19}$$

Equation 19 implies that the differentiation of the apparent shear rate corrected by wall slip with respect to shear stress is no longer equal to the non-Newtonian index of the fluid, which is assumed in the conventional Mooney method for a non-Newtonian fluid. Eliminating Q by introducing $\dot{\gamma}_a = 4Q/\pi R^3$ into Eq. 19, the shear rate at the wall can be obtained as:

$$\dot{\gamma}_w = \left(\dot{\gamma}_a - \frac{4u_s}{R}\right)\left[\frac{3 + d\ln\left(\frac{1}{4}\left(\dot{\gamma}_a - \frac{4u_s}{R}\right)\right)/d\ln\tau_w}{4}\right] \tag{20}$$

Equation 20 includes the Rabinowitsch correction for a non-Newtonian fluid with slip. Under no slip condition, i.e. $u_s = 0$, the usual Rabinowitsch correction for wall shear rate of a non-Newtonian fluid can be obtained:

$$\dot{\gamma}_w = \frac{\dot{\gamma}_a}{4}\left(3 + \frac{d\ln\dot{\gamma}_a}{d\ln\tau_w}\right) \tag{21}$$

The slip velocity of a non-Newtonian fluid was proposed as a power law function of wall shear stress[31]:

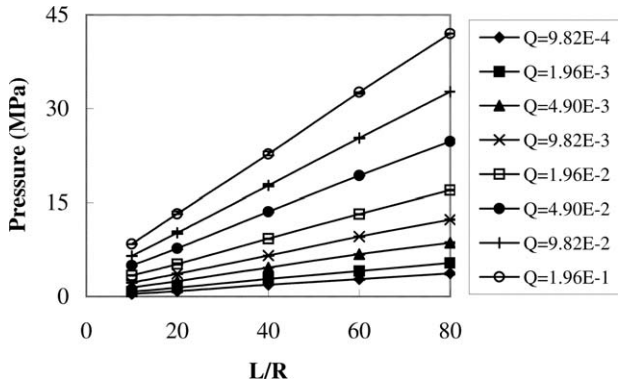

Figure 1. Bagley plot of pure EVA460 at 180°C for 1 mm die diameter (Q: cm^3/s).

$$u_s = \alpha \exp(\lambda T - \beta_p P)\tau_w^k \quad (22)$$

where α and λ are material constants, β_p is a coefficient related to pressure, typically of order 10^{-9} Pa^{-1}, P is the absolute pressure, k is a power-law index.

Equation 22 indicates that slip velocity increases with wall shear stress in the power-law function. However, this increase is reduced by the effect of pressure with a factor of $\exp(-\beta_p P)$. Thus, as the pressure becomes higher with increasing flow length, the effect of pressure on the slip velocity becomes more significant. The pressure-dependent wall slip was observed by others, see for example the recent investigations of Tang and Kalyon.[32,33] This implies that the slip velocity measured by dies with different ratio of die length to die radius (L/R) would be different. This conclusion agrees with the finding of Hatzikiriakos and Dealy.[4]

Experiments and Results

Materials and equipment

The polymer binder system is ethylene vinyl acetate (EVA) 460, manufactured by DUPONT under the trade name ELVAX, with a density of 941 kg/m^3 and a melt index of 1.8°/min. It was mixed homogenously with spherical glass particles (MO-SCI Corporation) with density 2500 kg/m^3 in a Haake Rheomix600 Torque Mixer with particle concentrations 35, 40, and 45% by volume. The investigated diameters of the spherical glass beads are in the range of 53–63 μm and 106–125 μm, respectively. The samples were dried in an oven. The preparation conditions for suspensions should be carefully selected and strictly observed to achieve reproducible characterization of rheological material functions.[34] In addition, in this investigation, repeatability was ensured by performing at least three tests for each testing condition.

To investigate the effect of temperature on wall slip, experiments were conducted at different temperatures (160, 180, and 210°C) on suspensions with particle size of 53–63 μm.

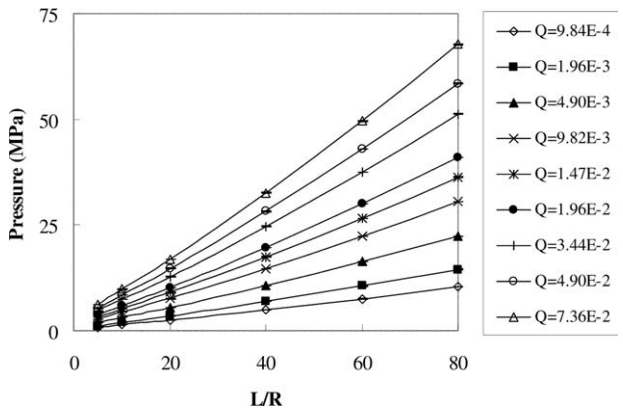

Figure 2. Bagley plot for concentrated suspension with ϕ = 40% for 1 mm die diameter at 180°C (Q: cm^3/s, 53–63 μm).

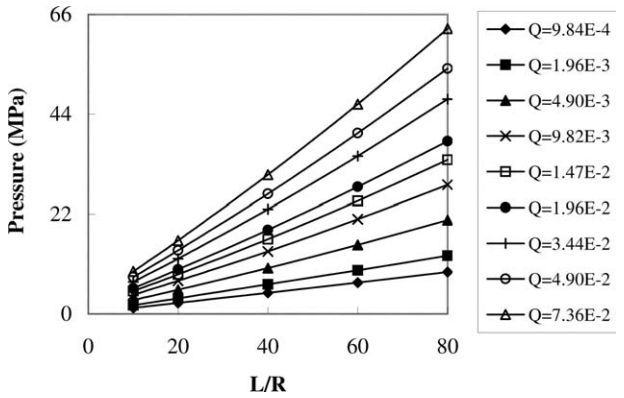

Figure 3. Bagley plot for concentrated suspension with ϕ = 40% for 1 mm die diameter at 180°C (Q: cm^3/s, 106–125 μm).

Entrance and exit losses

Bagley correction was conducted for flow experiments with different L/R ratios ranging from 5 to 80. To ensure consistency in the measurements, the dies for Bagley correction have the same diameter with a flat entry.

Figure 1 is the Bagley plot for pure EVA 460. Figures 2 and 3 are Bagley plots for concentrated suspensions with 40% particle concentration but with different particle sizes. All these plots were obtained using 1-mm diameter capillary dies at 180°C. The small error bars in the figures indicate that the repeatability of the measurements was good, with less than 4% difference between the experiments at the same conditions. The Bagley plot of pure EVA460 in Figure 1 shows good linearity. However, Figures 2 and 3 show that the nonlinearity is significant with an increasing flow rate for concentrated suspensions. These figures also show that even at the same flow rate, concentrated suspensions with the same particle concentration but different particle size, the pressure decreases with particle size. The end pressure due to entrance and exit losses can be determined by a quadratic fit to the Bagley plot,[5] i.e.

$$\Delta P = e_1(L/R)^2 + e_2(L/R) + \Delta P_e \quad (23)$$

where ΔP is the total measured pressure drop over the total length of the capillary, e_1 and e_1 are constants related to the flow rate, particle concentration and temperature. ΔP_e is the

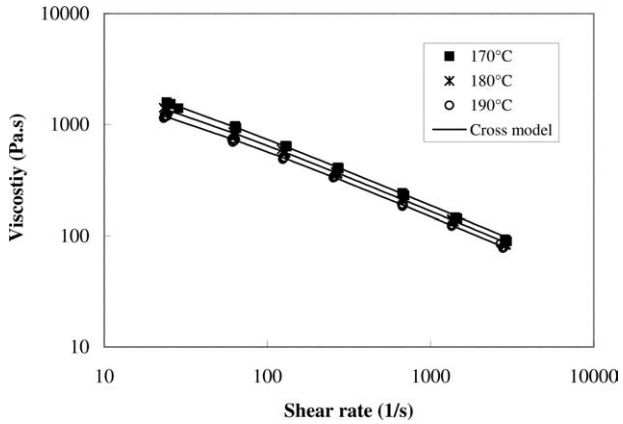

Figure 4. Viscosities of pure EVA460 and fitted modified Cross model at different temperatures.

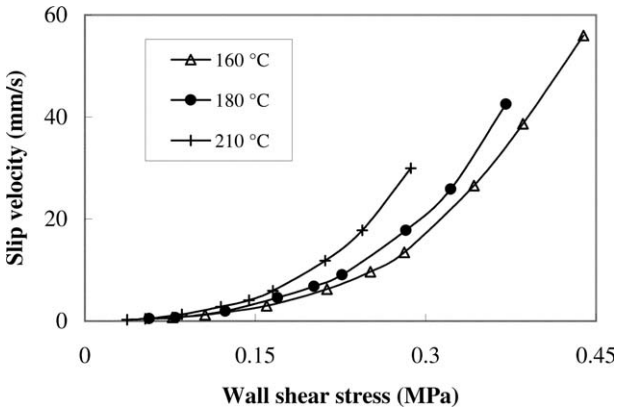

Figure 5. Slip velocities with 40% particle concentration with particle size 53–63 μm at different temperatures (160, 180, and 210°C).

entrance and exit losses. For pure binder, $e_1 = 0$ due to the linearity in the Bagley plot.

Viscosity of pure EVA 460

True viscosities of pure EVA 460 were obtained with Bagley and Rabinowitsch corrections at different temperatures, namely 170, 180, and 190°C, respectively. Figure 4 shows that the viscosity of EVA460 is shear thinning and decreases with increasing temperature. The modified Cross model can fit well the viscosity data. The standard error of fitted data with experimental data is negligible (only 0.18 Pa s). The material constants of EVA460 in the modified Cross model are listed in Table 1.

Wall slip

As slip behavior is related to the material of the die, the dies used in the measurement should all be of the same material with the same surface finish. Four different diameter dies with the same ratio of die length to radius ($L/R = 40$) were used in the capillary experiments. The die diameter was in the range of 0.5–1.25 mm (0.5, 0.75, 1, and 1.25 mm). These data allow the derivation of a Mooney plot for the analysis of the slip behavior of the suspension.

It is important to note that for each die diameter, the entrance and exit losses should be considered before calculating the slip velocity. As the entrance and exit losses are dependent on the contraction ratio between the barrel diameter and capillary diameter and particle concentration, significant error will result if the entrance and exit losses are not considered, especially for small dies.[31]

Figure 5 shows the slip velocity at three different temperatures (160, 180, and 210°C) with 40% particle concentration. With increasing temperature, the curve becomes steeper. The increase in slip velocity with an increase in temperature is principally related to the decrease of the viscosity of the binder. Figure 6 compares the slip velocities of concentrated suspensions with particles in different size ranges. The suspension with particle size in the range of 106–125 μm exhibited larger slip velocities compared with those with particle size in the range of 53–63 μm.

In addition to experimental investigations, the slip velocity is also calculated by numerical modeling according to the model proposed. As shown in Figure 7, the slip velocity for a specific L/R ratio is not uniform along the flow length, but increases from the inlet to the outlet. This increase is caused by the decrease in hydraulic pressure from the inlet to the outlet. Because of this nonuniformity, a length-averaged value is employed to characterize the slip velocity for a specific capillary. Figure 8 shows the slip velocities for various L/R ratios, which decreases with L/R. It indicates that the effect of pressure is dominant on the slip velocity with increasing flow length. These findings are in agreement with that of Kalika and Denn.[35] Figure 9 shows the comparison

Table 1. Material Constants of EVA460 in Modified Cross Model

A (Pa s)	1.14×10^{-2}
n	0.38
T_b (K)	5980
τ^* (Pa)	19860

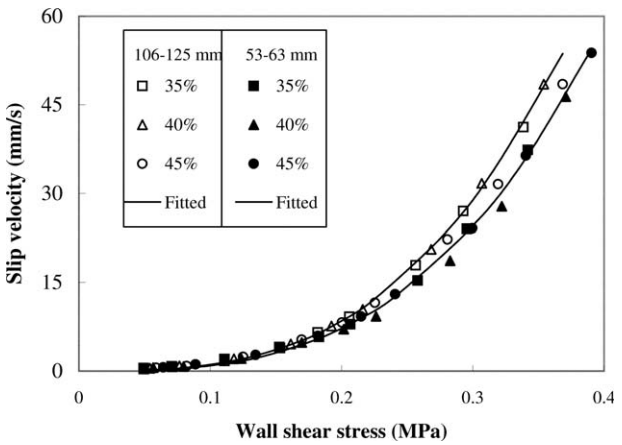

Figure 6. Slip velocities of concentrated suspensions with different particle concentrations and different particle sizes at 180°C (53–63 μm and 106–125 μm).

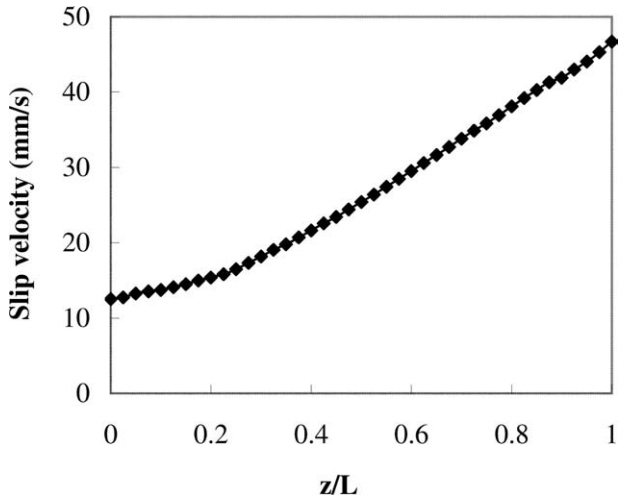

Figure 7. Slip velocity along the flow direction (Q = 7.36 × 10^{-2} cm^3/s, L/R = 40, R = 0.5 mm, ϕ = 40%, T = 180°C, 53–63 μm).

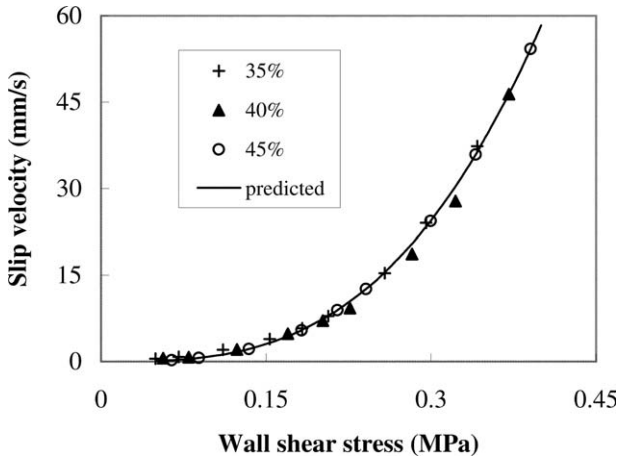

Figure 9. Comparison of slip velocity between numerical predictions and by the modified Mooney method (T = 180°C, L/R = 40, R = 0.5 mm, 53–63 μm).

of the slip velocities obtained by simulation and by experiments using the modified Mooney method for ratio L/R = 40. It is observed that they agree well, implying that the modified Mooney method can be used to determine the average slip velocity.

After obtaining the slip velocities at different temperatures, different pressures and different wall shear stresses, the constants in the slip model as described by Eq. 22 can be obtained by curve fitting. For the concentrated suspensions with particle size of 53–63 μm and 106–125 μm, the constants λ, β_p, and k are the same, but α changes with particle size, see Table 2.

True viscosity of concentrated suspension

Subsequent to the corrections of slip velocity and entrance and exit losses, the true viscosity of a concentrated suspension can be calculated by:

$$\tau_w = \frac{P - \Delta P_e}{2L/R} \tag{24}$$

$$\eta = \frac{\tau_w}{\dot{\gamma}_w} \tag{25}$$

The corrected shear rate at the wall $\dot{\gamma}_w$ is obtained by Eq. 20 based on Mooney plot, in which the wall slip, u_s, is determined at different corrected wall shear stress, τ_w, obtained by Eq. 24.

Figures 10 and 11 summarize the viscosities of pure EVA and concentrated suspensions with three particle concentrations and different particle sizes at 180°C. In terms of Krieger model,[25] the relationship of viscosity with shear rate at different particle concentrations can be expressed as:

$$\eta = \eta_b\left(1 - \frac{\phi}{\phi_c}\right)^{-m} = \frac{\eta_0}{1 + (\eta_0\dot{\gamma}/\tau^*)^{1-n}}\left(1 - \frac{\phi}{\phi_c}\right)^{-m} \tag{26}$$

The constants m in Eq. 26 together with k_c and k_η in Eq. 12 were determined, see Appendix C. The extended Krieger model (26) is an empirical model describing the shear deformation and concentration dependent viscosity. For suspensions with the same particle concentration but with particles in different particle size range, their viscosities are not the same even with the same ϕ and tested at the same conditions (shear rate, etc.). The change of viscosity with particle size may be reflected in the changes of m and ϕ_c. It should be noted that due to particle migration, the value of particle concentration ϕ in Eq. 26 is no longer the

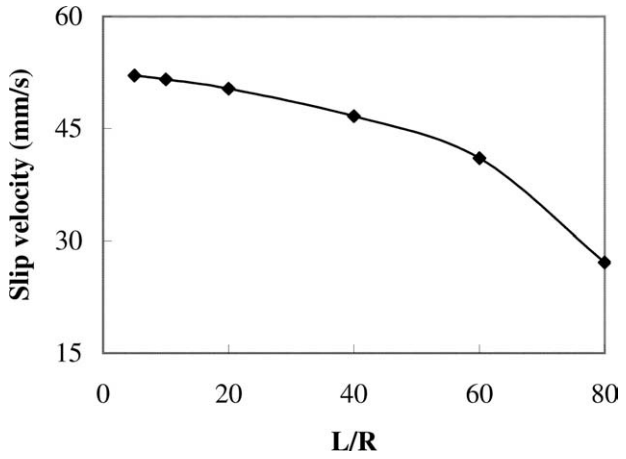

Figure 8. Average slip velocity vs. L/R (Q = 7.36 × 10^{-2} cm^3/s, R = 0.5 mm, ϕ = 40%, T = 180°C, 53–63 μm).

Table 2. Constants in Slip Model

Constants	53–63 μm	106–125 μm
α (mm/s)	2.14	2.69
λ (1/K)	0.013	0.013
β_p (1/Pa)	1.5 × 10^{-9}	1.5 × 10^{-9}
k	3.03	3.03

initial concentration of feedstock, but an effective concentration. It has to be obtained by numerical calculation taking into consideration particle migration.[28]

For particle sizes range between 53–63 μm and 106–125 μm, $m = 1.28$ and $m = 1.08$, respectively. Thus, m decreases with increasing particle size, implying that a concentrated suspension with the same particle concentration but larger particles has a lower viscosity than that with smaller particles. This is probably due to the larger number of particles in the concentrated suspension with smaller particle size for the same particle concentration (measured in total volume). A larger number of particles will result in more particle–particle interactions and an increased resistance to flow, resulting in a larger viscosity. This is reflected in the Krieger model with the value of m decreasing with increasing particle size.

The value of ϕ_c depends on the uniformity of particle size, the effective microstructure of the packed configuration and the type of flow. For uniform diameter particles, the value of ϕ_c can vary over a range from 0.52 (simple cubic packing) to 0.74 (face-centered cubic packing).[25] Still other values of ϕ_c are applicable to randomly packed particles and bimodal suspensions. Although the studied particles are in different size ranges, namely 53–63 μm and 106–125 μm, respectively, they can be regarded to be in the same order of magnitude. As both are of spherical shapes, the same value of $\phi_c = 68\%$ may be assumed for both. This critical volume percentage was also employed by Subia et al.[36] to spherical particles. Indeed, our experimental data indicate that for our system, the effect of particle size on viscosity is dominantly reflected by the change of the value of m, and not by ϕ_c.

Conclusion

Corrections for the true viscosities of concentrated suspensions with capillary rheometer were investigated, which includes the corrections of end effects, Rabinowitsch effect and wall slip. For end effect corrections, an entrance and exit losses model was formulated which combines the effects of particle concentration, the contraction ratio and temperature. For slip correction, a slip model was developed which takes into account the non-Newtonian viscosity and the nonlinearity of slip velocity on wall shear stress. The effective particle concentration with particle migration is calculated by a diffusive numerical model. It is found that Bagley plots of concentrated suspensions are nonlinear due to particle migration and wall slip. Slip velocity increases with increasing particle size and decreasing temperature. Particle size was found to affect significantly the viscosity of the suspension with viscosity decreasing with increasing particle size, which can be reflected by a decrease in value of the power-law index in the Krieger model.

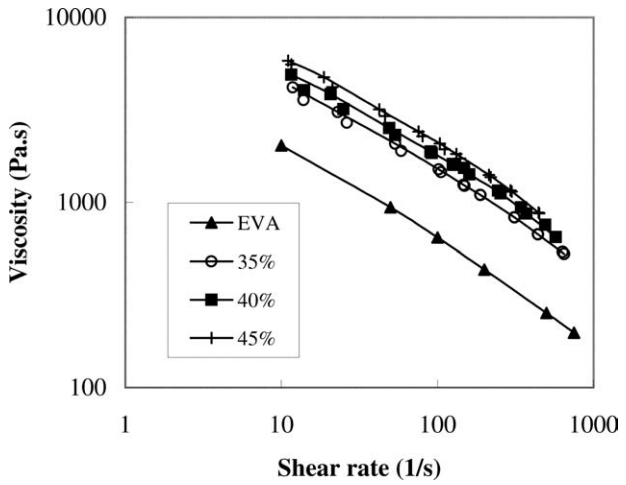

Figure 10. True viscosities of pure EVA and suspensions with different particle concentrations at 180°C (53–63 μm).

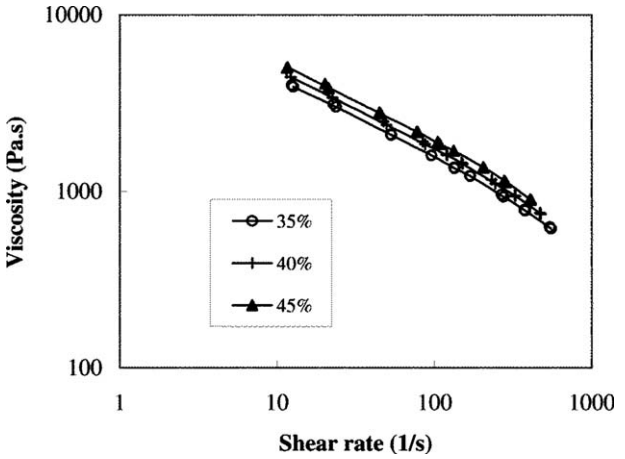

Figure 11. True viscosities of suspensions with different particle concentrations at 180°C (106–125 μm).

Literature Cited

1. Barnes HA. A review of the rheology of filled viscoelastic systems. In: Binding DM, Walters K, editors. *Rheology Reviews*. United Kingdom: British Society of Rheology, 2003:1–36.
2. Bagley EB. End correction in the capillary flow of polyethylene. *J Appl Phys*. 1957;28:624–627.
3. Laun HM, Schuch H. Transient elongational viscosities and drawability of polymer melts. *J Rheol*. 1989;33:119–175.
4. Hatzikiriakos SG, Dealy JM. Wall slip of molten high density polyethylenes. II. Capillary rheometer studies. *J Rheol*. 1992;36:703–741.
5. Macosko, CM. *Rheology, Principles, Measurements, and Applications*. VCH: New York, 1994.
6. Kalyon DM. Apparent slip and viscoplasticity of concentrated suspensions. *J Rheol*. 2005;49:641–640.
7. Vand V. Viscosity of solutions and suspensions. I. Theory. *J Phys Chem*. 1948;52:277–299.
8. Gadala-Maria F, Acrivos A. Shear-induced structure in a concentrated suspension of solids sphere. *J Rheol*. 1980;24:799–811.
9. Graham AL, Altobelli SA, Fukushima E, Mondy LA, Stephen TS. NMR Imaging of shear-induced diffusion and structure in concentrated suspensions undergoing Couette flow. *J Rheol*. 1991;35: 191–201.
10. Koh CJ, Hookham P, Leal LG. An experimental investigation of concentrated suspension flows in a rectangular channel. *J Fluid Mech*. 1994;266:1–31.
11. Jana S, Kapoor B, Acrivos A. Apparent wall-slip velocity coefficients in concentrated suspensions of noncolloidal particles. *J Rheol*. 1995;39:1123–1132.
12. Leighton D, Acrivos A. The shear-induced migration of particles in concentrated suspensions. *J Fluid Mech*. 1987;181:415–439.

13. Phillips RJ, Armstrong RC, Brown RA, Graham AL, Abbot JR. A constitutive equations for concentrated suspensions that accounts for shear-induced particle migration. *Phys Fluids A*. 1992;4:30–40.
14. Miller RM, Morris JF. Normal stress-driven migration and axial development in pressure-driven flow of concentrated suspensions. *J Non-Newtonian Fluid Mech*. 2006;135:149–165.
15. Mooney M. Explicit formula for slip and fluidity. *J Rheol*. 1931; 2:210–222.
16. Yilmazer U, Kalyon DM. Dilatancy of concentrated suspensions with Newtonian matrices. *Polym Compos*. 1991;12:226–232.
17. Kalyon D. Letter to the editor: comments on 'A new method of processing capillary viscometry data in the presence of wall slip'. *J Rheol*. 2003;47:337–348, 187–1088.
18. Oldroyd JC. The interpretation of observed pressure gradients in laminar flow of non-Newtonian liquids through tubes. *Colloid Sci*. 1949;4:333–342.
19. Jastrzebski ZD. Entrance effects and wall effects in an extrusion rheometer during the flow of concentrated suspensions. *Ind Eng Chem Fund*. 1967;6:445–454.
20. Martin PJ, Wilson DJ. A critical assessment of the Jastrzebski interface condition for the capillary flow of pastes, foams, and polymers. *Chem Eng Sci*. 2005;60:493–502.
21. Bird RB, Stewart WE, Lightfoot EN. *Transport Phenomena*. Wiley: New York, 1960.
22. Miller RM, Morris JF. Normal stress-driven migration and axial development in pressure-driven flow of concentrated suspensions. *J non-Newtonian Fluid Mech*. 2006;135:149–165.
23. Batchelor GK, Green JT. The determination of the bulk stress in a suspension of spherical particles and diffusion. *J Fluid Mech*. 1972;56:401–427.
24. Jeffrey DJ, Acrivos A. The rheological properties of suspensions of rigid particles. *J AIChE*. 1976;22:417–432.
25. Krieger IM. Rheology of monodisperse lattices. *Adv Colloid Interface Sci*. 1972;3:111–136.
26. Chen X, Lam YC, Tan KW, Chai JC, Yu SCM. Shear-induced particle migration modelling in a concentrated suspension flow. *Model Simul Mater Sci*. 2003;11:503–522.
27. Graham AL, Mammoli AA, Busch MB. Effects of demixing on suspension rheometry. *Rheol Acta*. 1998;37:139–150.
28. Chen X, Lam YC, Wang ZY, Tan KW. Determination of phenomenological constants of shear-induced particle migration model. *Comp Mater Sci*. 2004;30:223–229.
29. Wang ZY, Sunil JC, Lam YC, Chen X. End pressure corrections in capillary rheometry of concentrated suspensions. *J Appl Polym Sci*. 2009;114:1738–1745.
30. Barnes HA. A review of the wall slip (wall depletion) of polylmer-solutions, emulsions and particle suspension in viscometers-its cause,-character, and cure. *J Non-Newtonian Fluid Mech*. 1995;56: 221–251.
31. Lam YC, Wang ZY, Chen X, Joshi SC. Wall slip of concentrated suspension melts in capillary flows. *Powder Technol*. 2007;177:162–169.
32. Tang HS, Kalyon DM. Time-dependent tube flow of compressible suspensions subject to pressure dependent wall slip: ramifications on development of flow instabilities. *J Rheol*. 2008;52:1069–1090.
33. Tang HS, Kalyon DM. Unsteady circular tube flow of compressible polymeric liquids subject to pressure-dependent wall slip. *J Rheol*. 2008;52:507–525.
34. Kalyon DM, Dalwadi D, Erol M, Birinci E, Tsenoglu C. Rheological behavior of concentrated suspensions as affected by the dynamics of the mixing process. *Rheol Acta*. 2006;45:641–658.
35. Kalika DS, Denn MM. Wall slip and extrudate distortion in linear low-density polyethylene. *J Rheol*. 1987;31:815–834.
36. Subia SR, Ingber MS, Mondy A, Altobelli SA, Graham AL. Modelling of concentrated suspensions using a continuum constitutive equation. *J Fluid Mech*. 1998;373:193–219.

Appendix A: Solution for Nonlinear Pressure Equation

Based on the lubrication approximation theory, the simplified flow equations for a concentrated suspension in a capillary tube is:

$$\frac{\partial P}{\partial z} - \frac{1}{r}\frac{\partial}{\partial r}\left(r\eta\frac{\partial u}{\partial r}\right) = 0 \tag{A1}$$

By introducing the Krieger model (5) and the modified cross viscosity model (6) for a polymeric binder into Eq. A1, the shear rate equation can be written as:

$$\left(\frac{\dot{\gamma}}{\dot{\gamma}_0}\right) - \frac{\Lambda_z r}{2\tau*}\left(1-\frac{\phi}{\phi_c}\right)^m\left[1+\left(\frac{\dot{\gamma}}{\dot{\gamma}_0}\right)^{1-n}\right] = 0 \tag{A2}$$

where $\Lambda_z = \frac{\partial P}{-\partial z}$ is the pressure gradient along the flow direction.

A numerical method, namely the finite volume method, was employed for solving Eq. A2. By dividing the radius into N intervals, the shear rate at the node i, $\dot{\gamma}_{i,j}$ can be determined by the following N equations:

$$\left(\frac{\dot{\gamma}_{i,j}}{\dot{\gamma}_0}\right) - \frac{\Lambda_{zi} r_{i,j}}{2\tau*}\left(1-\frac{\phi_{i,j}}{\phi_c}\right)^m\left\{\left(\frac{\dot{\gamma}_{i,j}}{\dot{\gamma}_0}\right)^{1-n}+1\right\} = 0 \quad (j=1,\ldots,N) \tag{A3}$$

The interval halving method can be employed for solving this nonlinear equation. When the slip boundary condition is employed at the wall, the total volumetric flow rate Q can be expressed as:

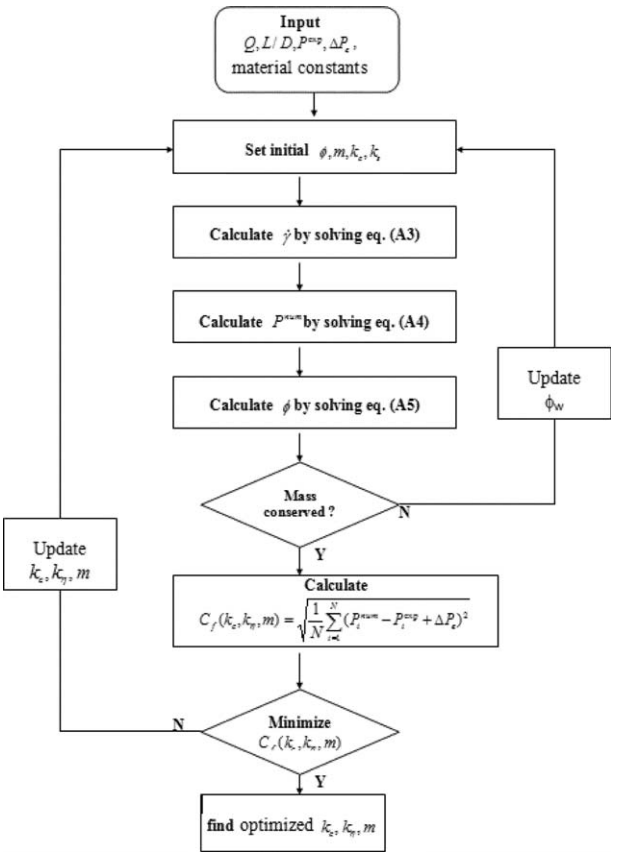

Figure C1. Flow chart for determination of k_c, k_η, and m.

$$Q = Q_{\text{slip}} + Q_{\text{vis}} = \alpha\pi R^2 \exp\left(\lambda T - \beta_{\text{p}} P_i\right)\left(\frac{\Lambda_{zi} R}{2}\right)^k + \pi \int_0^R \dot{\gamma}_{i,j} r^2 dr \quad \text{(A4)}$$

Equations A3 and A4 are coupled nonlinear systems of equations for pressure gradient field and shear rate. This requires an under-relaxation iteration procedure to obtain a convergent numerical solution. Estimates of Λ_z can be obtained by solving Eq. A4 with an initial value of $\dot{\gamma}_{i,j}$. Subsequently, shear rate $\dot{\gamma}_{i,j}$ can be determined by solving Eq. A3. Subsequently, a more accurate estimate of Λ_z can be obtained by solving Eq. A4 again. This iteration procedure is repeated until a converged solution is obtained. In our calculations, the initial guesses of $\dot{\gamma}_{i,j}$ are obtained from the power-law model.

Appendix B: Solution for Particle Concentration

To solve the diffusive Eq. 12 by finite volume method, the discretization scheme of diffusive Eq. 12 can be described as follows:

$$B_{i,j}\phi_{i,j+1,t+\Delta t} + A_{i,j}\phi_{i,j,t+\Delta t} + C_{i,j}\phi_{i,j-1,t+\Delta t} = \psi \quad \text{(B1)}$$

where

$$B_{i,j} = \Delta z \cdot \Delta t \cdot w \cdot a^2 \left\{ (j+1)\dot{\gamma}_{i,j+1,t}\left[k_{\text{c}}\phi_{i,j+1,t} + \frac{m k_{\text{s}} \phi_{i,j+1,t}^2}{\phi_{\text{c}} - \phi_{i,j+1,t}}\right] + j \cdot \dot{\gamma}_{i,j,t}\left[k_{\text{c}}\phi_{i,j,t} + \frac{m k_{\text{s}} \phi_{i,j,t}^2}{\phi_{\text{c}} - \phi_{i,j,t}}\right]\right\}$$

$$A_{i,j} = \Delta z \cdot \Delta t \cdot w \cdot a^2 \left\{ (j+1)\dot{\gamma}_{i,j+1,t}\left[k_{\text{c}}\phi_{i,j+1,t} + \frac{m k_{\text{s}} \phi_{i,j+1,t}^2}{\phi_{\text{c}} - \phi_{i,j+1,t}}\right] + 2j \cdot \dot{\gamma}_{i,j,t}\left[k_{\text{c}}\phi_{i,j,t} + \frac{m k_{\text{s}} \phi_{i,j,t}^2}{\phi_{\text{c}} - \phi_{i,j,t}}\right] + (j-1) \cdot \dot{\gamma}_{i,j-1,t}\left[k_{\text{c}}\phi_{i,j-1,t} + \frac{m k_{\text{s}} \phi_{i,j-1,t}^2}{\phi_{\text{c}} - \phi_{i,j-1,t}}\right]\right\} + 2\Delta r^2 \times j(\Delta x + u_{i,j,t} \cdot \Delta t)$$

$$C_{i,j} = \Delta z \cdot \Delta t \cdot w \cdot a^2 \left\{ (j-1)\dot{\gamma}_{i,j-1,t}\left[k_{\text{c}}\phi_{i,j-1,t} + \frac{m k_{\text{s}} \phi_{i,j-1,t}^2}{\phi_{\text{c}} - \phi_{i,j-1,t}}\right] + j \cdot \dot{\gamma}_{i,j,t}\left[k_{\text{c}}\phi_{i,j,t} + \frac{m k_{\text{s}} \phi_{i,j,t}^2}{\phi_{\text{c}} - \phi_{i,j,t}}\right]\right\}$$

$$\psi = 2\Delta r^2 \cdot j \cdot \phi_{i-1,j,t}[\Delta z - u_{i,j,t} \cdot (1-\vartheta) \cdot \Delta t] + 2\Delta r^2 \cdot j \cdot \Delta t + \Delta z \cdot \Delta t \cdot (1-w) \cdot a^2 \left\{ (j-1)\dot{\gamma}_{i,j-1,t}\left[k_{\text{c}}\phi_{i,j-1,t} + \frac{m k_{\text{s}} \phi_{i,j-1,t}^2}{\phi_{\text{c}} - \phi_{i,j-1,t}}\right] + (j+1)\dot{\gamma}_{i,j+1,t}\left[k_{\text{c}}\phi_{i,j+1,t} + \frac{m k_{\text{s}} \phi_{i,j+1,t}^2}{\phi_{\text{c}} - \phi_{i,j+1,t}}\right] - 2j \cdot \dot{\gamma}_{i,j,t}\left[k_{\text{c}}\phi_{i,j,t} + \frac{m k_{\text{s}} \phi_{i,j,t}^2}{\phi_{\text{c}} - \phi_{i,j,t}}\right]\right\} + \frac{k_{\text{c}}\pi\Delta z\Delta t}{\Delta r}\left\{\left[(j+1)\phi_{i,j+1,t} + j\phi_{i,j,t}\right]\dot{\gamma}_{i,j+1,t} + \left[(j-1)\phi_{i,j-1,t} + j\phi_{i,j,t}\right]\dot{\gamma}_{i,j-1,t} - \left[(j+1)\phi_{i,j+1,t} + 2j\phi_{i,j,t} + (j-1)\phi_{i,j-1,t}\right]\dot{\gamma}_{i,j,t}\right\}$$

If $w = 1/2$, it is the Crank–Nicolson scheme. This means that the concentration at time t and $t + \Delta t$ are equally weighted. The system of algebraic equations of Eq. B1 is a tridiagonal-matrix, which can be solved by Thomas algorithm[26] at each time level. The procedure is repeated to progress the solution for a further time step.

Appendix C: Determination of Power-Law Index, m, in Krieger Model, and k_{c}, k_η in Diffusive Flux Model

The cost or objective function can be written as the sum of squares of differences between the measured and predicted pressures taking into consideration pressure loss due to end effect.

$$C_{\text{f}}(k_{\text{c}}, k_\eta, m) = \sqrt{\frac{1}{N}\sum_{i=1}^{N}\left(P_i^{\text{num}} - P_i^{\text{exp}} + \Delta P_{\text{e}}^{\text{exp}}\right)^2} \quad \text{(C1)}$$

The main calculation steps are outlined in Figure C1.

Manuscript received Nov. 7, 2008, and revision received Aug. 5, 2009.